Convective heat transfer of nanofluid in a wavy channel: Buongiorno's mathematical model

N. Shehzad [a], A. Zeeshan [a], R. Ellahi [a,b,*], K. Vafai [b]

[a] Department of Mathematics and Statistics, FBAS, IIIUI, Islamabad, Pakistan
[b] Department of Mechanical Engineering, University of California Riverside, USA

ABSTRACT

The present article addresses the effects of convective heat transfer of nanofluid utilizing Buongiorno's model in a wavy channel. The simultaneous effects of Brownian motion and thermophoresis are discussed. The solutions for velocity, temperature and concentration are analytically obtained. Effects of sundry parameters such as Lewis number Le, Prandtl number Pr, thermophoresis number Nt and Brownian motion number Nb are graphically presented. The streamlines have also been shown to discuss the skin fiction with the different buoyancy discipline. Computations for hybrid Genetic Algorithm and Nelder-Mead approach are also offered for the validity of obtained results.

© 2016 Elsevier B.V. All rights reserved.

1. Introduction

New resources to improve the heat transfer characteristics are very much needed for increasing the efficiency for making significant energy savings in industry. The main crises are due to the low thermal conductivity of the conventional liquids used in square enclosures such as, water, oil, acetone, ethylene and glycol. An advanced technique for improving heat transfer characteristics is to use solid particles in nanoscale (smaller than 100 nm) in working liquids. This technique has already been used extensively over the past one decade. It is found that the heat exchange can be upgraded by presenting nanoparticles with high thermal properties in low volume fraction within the liquid that leads to new-fangled category of fluids named as nanofluids [1]. Nanofluid refers to the fluid suspension of nanosize particles having less than 100 nm dimension in the base fluid whereas the base fluid, or dissolving medium, can be aqueous or non-aqueous in nature and nanoparticles are metals, carbides, oxides, carbon nanotubes or nitrides and nanoparticles shapes may be disks, spheres, or rods, etc. [2]. Nanoparticles are better to enhance the thermal conductivity of fluid in nature but not sufficient condition for obtaining high-performance in heat exchanging equipment, therefor further investigation is required in this field. Many researchers have investigated the effect of nanofluid on heat transfer enhancement and thermal conductivities of different shapes of nanoparticles like spherical and non-spherical are of great interest in various engineering applications which strongly suggest that

nanoparticle plays a significant role in the thermal transport in nanofluids [3–14].

Moreover, fluid flow with convection has many applications in the industrial and engineering processes such as thermal designing of buildings, drying of porous solid and solar power collector. Recently, in the wavy channels convective flow has received great attention. When fluid flows in wavy channels, then the collaboration of fluid enhanced the heat transfer rate near the wavy walls. The fluid flow and heat transfer in corrugated channel with various models using traditional fluids as base fluids have been examined by many researchers [15–20]. They have observed that an increase in the pressure drop always enhances the heat transfer flow in straight channel. In particular, large particles in the fluid quickly settle out of suspension and passing through micro channels cause severe blockage and increase the pressure considerably [21]. In the experimental investigation on the suspension of 4.0% volume 35 nm CuO particles in ethylene glycol, Lee et al. [22] examined 20% increase in thermal conductivity. Xuan and Li [23,24] have examined experimentally thermal conductivity and conductivity heat transfer feature and flow performance of copper-water nanofluid. It was found that the nanoparticles extraordinarily improve heat transfer performance of the base fluid. Santra et al. [25] numerically studied the heat transfer feature of copper-water nanofluid in a two-dimensional horizontal duct. It was detected that with the increase of nanoparticle volume fraction, heat transfer flow rate increases. Noreen [26] also analytically discussed the nanofluid in a symmetric channel and so forth.

Furthermore, fluid flow is governed by the nonlinear coupled partial differential equation system of mass, momentum, energy conservation and concentration of nanofluid. The flow of nonlinear fluids has gained noteworthy significance owing to its several applications in the fields of

---

* Corresponding author.
E-mail addresses: rellahi@engr.ucr.edu, rahmatellahi@yahoo.com (R. Ellahi).

applied science and engineering. The traditional Navier-Stokes equations are not adequate to foresee the features of such flows. Generally mathematical formulation for such fluids is much complicated. Due to nonlinear coupled equations, the case becomes quite complex. Homtopic procedure [27,28] is utilized for the solutions of arising nonlinear differential systems. Solutions of homotopy technique are also optimized by using optimization technique along with minimize residual error which are very rare in the literature. Combinations of optimization technique gave the tremendous solutions. Results for velocity, temperature, Nusselt number, skin-friction coefficient, and Sherwood number in this investigation are investigated at 30th order iterations.

The main objective of the present study is to examine the convective heat transfer of nanofluid in a wavy channel with constant pressure gradient. The investigation covers Reynolds number in between the range 0 to 1 whereas nanoparticle volume fraction lies in the range of (0–1) %. Firstly development of the problem is given in the next section. Secondly, efforts are devoted to find analytical solutions in Section 2. Thirdly to examine the validity of obtained results, convergence of solutions is discussed in Section 3 with hybrid techniques. The mechanical properties of reported study are presented in Section 4 through pictorial and numerical tables. Finally, Section 5 summarized the conclusions.

2. Development of problem

The two-dimensional steady boundary layer flow of a nanofluid through the horizontal symmetric channel bounded by two wavy walls is considered. Fluid is driven by constant pressure gradient and Buoyancy force. Here consider the $\overline{x}$-axis along the direction of the flow and $\overline{y}$-axis is perpendicular to it. Let us consider the wavy walls $H_1 = -d - a\text{Cos}(\frac{2\pi}{L}\overline{x})$ and $H_2 = d + a\text{Cos}(\frac{2\pi}{L}\overline{x})$. We assume that the wavelength λ of the wavy walls, which is proportional to $\frac{2\pi}{L}$ is large, where a is wave amplitude of wavy wall, d is the mean width of the channel and L is the length of wavy channel (Fig. 1).

The following four field equations represent the conservation of total mass, momentum, thermal energy and nanoparticles, respectively. The field variables are the velocity $\overline{V}$, the temperature $\overline{T}$ and nanoparticle concentration $\overline{C}$.

$$\nabla.\overline{V} = 0, \tag{1}$$

$$\rho_f\left(\frac{\partial\overline{V}}{\partial\overline{t}} + \overline{V}.\nabla\overline{V}\right) = -\nabla\overline{p} + \mu\nabla^2\overline{V} + \left[\overline{C}\rho_p + \left(1-\overline{C}\right)\left\{\rho_f\left(1-\beta(\overline{T}-T^*)\right)\right\}\right]\boldsymbol{g}, \tag{2}$$

$$(\rho C)_f\left(\frac{\partial\overline{T}}{\partial\overline{t}} + \overline{V}.\nabla\overline{T}\right) = K\nabla^2\overline{T} + (\rho C)_p\left[D_B\nabla C.\nabla\overline{T} + (D_T/T*)\nabla\overline{T}.\nabla\overline{T}\right] + \Phi, \tag{3}$$

$$\frac{\partial\overline{C}}{\partial\overline{t}} + \overline{V}.\nabla\overline{C} = D_B\nabla^2\overline{C} + (D_T/T*)\nabla^2\overline{T}. \tag{4}$$

Where $\overline{V} = (\overline{u},\overline{v})$ is the velocity, $\overline{u}, \overline{v}$ are the velocity components in the $\overline{x}, \overline{y}$ directions, ρ_f is the density of the base fluid, $\overline{p}$ is the pressure, μ is the viscosity, K is the thermal conductivity, $(\rho C)_f$ is the heat capacity of fluid, $(\rho C)_p$ is the effective heat capacity of nanoparticle material, Φ is the viscous dissipation, β is the volumetric volume expansion coefficient of the nanofluid and ρ_p is the density of the particles. T^* is the mean value of T_1 and T_2, C^* is the mean value of C_1 and C_2, $\boldsymbol{g}$ is the gravitational acceleration, D_B is the Brownian diffusion coefficient and D_T is the thermophoretic diffusion coefficient [29,30].

Governing equations in components form can be written as

$$\frac{\partial\overline{u}}{\partial\overline{x}} + \frac{\partial\overline{v}}{\partial\overline{y}} = 0, \tag{5}$$

$$\rho_f\left(\overline{u}\frac{\partial\overline{u}}{\partial\overline{x}} + \overline{v}\frac{\partial\overline{u}}{\partial\overline{y}}\right) = -\frac{\partial\overline{p}}{\partial\overline{x}} + \mu\left(\frac{\partial^2\overline{u}}{\partial\overline{x}^2} + \frac{\partial^2\overline{u}}{\partial\overline{y}^2}\right) + \left[\left(\rho_p-\rho_f\right)\left(\overline{C}-C^*\right) + (1-C^*)\rho_f\beta(\overline{T}-T^*)\right]g, \tag{6}$$

$$\rho_f\left(\overline{u}\frac{\partial\overline{v}}{\partial\overline{x}} + \overline{v}\frac{\partial\overline{v}}{\partial\overline{y}}\right) = -\frac{\partial\overline{p}}{\partial\overline{y}} + \mu\left(\frac{\partial^2\overline{v}}{\partial\overline{x}^2} + \frac{\partial^2\overline{v}}{\partial\overline{y}^2}\right) + \left[\left(\rho_p-\rho_f\right)\left(\overline{C}-C^*\right) + (1-C^*)\rho_f\beta(\overline{T}-T^*)\right]g, \tag{7}$$

$$\overline{u}\frac{\partial\overline{T}}{\partial\overline{x}} + \overline{v}\frac{\partial\overline{T}}{\partial\overline{y}} = \alpha\left(\frac{\partial^2\overline{T}}{\partial\overline{x}^2} + \frac{\partial^2\overline{T}}{\partial\overline{y}^2}\right) + \tau\left[D_B\frac{\partial\phi}{\partial\overline{y}}\frac{\partial\overline{T}}{\partial\overline{y}} + \frac{D_T}{T*}\left(\frac{\partial\overline{T}}{\partial\overline{y}}\right)^2\right] + \frac{\mu}{(\rho C)_p}\left(\frac{\partial\overline{u}}{\partial\overline{y}}\right)^2, \tag{8}$$

$$\overline{u}\frac{\partial\overline{C}}{\partial\overline{x}} + \overline{v}\frac{\partial\overline{C}}{\partial\overline{y}} = D_B\frac{\partial^2\overline{C}}{\partial\overline{y}^2} + \left(\frac{D_T}{T*}\right)\frac{\partial^2\overline{T}}{\partial\overline{y}^2} \tag{9}$$

Where α is the thermal diffusivity, $\alpha = \frac{K}{(\rho C)_f}$ and τ is parameter defined by $\tau = \frac{(\rho C)_p}{(\rho C)_f}$.
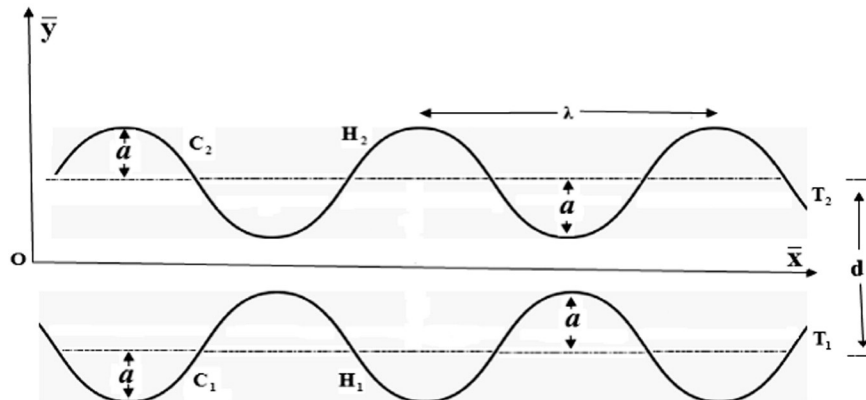

Fig. 1. Schematic diagrams of the physical model.

With boundary conditions

$$\bar{u} = 0, \bar{v} = 0, \bar{T} = T_1, \bar{C} = C_1 \text{ at } \bar{y} = H_1$$
$$\bar{u} = 0, \bar{T} = T_2 \text{ at } \bar{y} = H_2. \tag{10}$$

In order to convert the governing equations and the boundary conditions into a dimensionless form, the following dimensionless variables are introduced:

$$x = \frac{\bar{x}}{\lambda}, y = \frac{\bar{y}}{d}, u = \frac{\bar{u}}{c}, v = \frac{\bar{v}}{c\delta}, \delta = \frac{d}{\lambda}, p = \frac{d^2\bar{p}}{\mu c \lambda}, h_1 = \frac{H_1}{d},$$
$$h_2 = \frac{H_2}{d}, \text{Re} = \frac{\rho c d}{\mu}, \theta = \frac{\bar{T}-T^*}{T_1-T^*}, n = \frac{T_2-T^*}{T_1-T^*}, \phi = \frac{\bar{C}-C^*}{C_1-C^*}, \tag{11}$$
$$m = \frac{C_2-C^*}{C_1-C^*}, \text{Pr} = \frac{C_p\mu}{K}, Le = \frac{\alpha}{D_B}, S_c = \text{Pr} Le = \frac{\mu}{\rho D_B}.$$

Where Pr is the Prandtl number, Re is the Reynolds number, δ is the dimensionless wave number, c is the constant speed of channel walls, Le is the Lewis number, S_c is the Schmidt number, θ dimensionless temperature, ϕ is the concentration, n is the temperature scale, governing the variable temperature-difference between the two channel walls and m is the concentration scale, governing the variable concentration-difference between the two channel walls.

In view of Eq. (11), Eqs. (5) to (9) in dimensionless can be expressed:

$$\frac{\partial u}{\partial x} + \frac{\partial v}{\partial y} = 0, \tag{12}$$

$$\text{Re}\delta\left(u\frac{\partial u}{\partial x} + v\frac{\partial u}{\partial y}\right) = -\frac{\partial p}{\partial x} + \left(\delta^2\frac{\partial^2 u}{\partial x^2} + \frac{\partial^2 u}{\partial y^2}\right) + \left[(\rho_p-\rho_f)(C_1-C^*)\phi + (1-C^*)\rho_f\beta(T_1-T^*)\theta\right]g, \tag{13}$$

$$\text{Re}\delta^3\left(u\frac{\partial v}{\partial x} + v\frac{\partial v}{\partial y}\right) = -\frac{\partial p}{\partial y} + \delta^2\left(\delta^2\frac{\partial^2 v}{\partial x^2} + \frac{\partial^2 v}{\partial y^2}\right) + \left[(\rho_p-\rho_f)(C_1-C^*)\phi + (1-C^*)\rho_f\beta(T_1-T^*)\theta\right]g, \tag{14}$$

$$\text{RePr}\delta\left(u\frac{\partial\theta}{\partial x} + v\frac{\partial\theta}{\partial y}\right) = \left(\delta^2\frac{\partial^2\theta}{\partial x^2} + \frac{\partial^2\theta}{\partial y^2}\right) + \frac{\tau D_B(C_1-C^*)}{\alpha}\frac{\partial\phi}{\partial y}\frac{\partial\theta}{\partial y} + \frac{\tau D_T(T_1-T^*)}{\alpha T^*}\left(\frac{\partial\theta}{\partial y}\right)^2 + \frac{\mu c^2}{\alpha(T_1-T^*)(\rho C)_p}\left(\frac{\partial u}{\partial y}\right)^2, \tag{15}$$

$$\text{Re}\delta\left(u\frac{\partial\phi}{\partial x} + v\frac{\partial\phi}{\partial y}\right) = \frac{1}{S_c}\left[\left(\delta^2\frac{\partial^2\phi}{\partial x^2} + \frac{\partial^2\phi}{\partial y^2}\right) + \frac{D_T(T_1-T^*)}{D_B(C_1-C^*)}\left(\delta^2\frac{\partial^2\theta}{\partial x^2} + \frac{\partial^2\theta}{\partial y^2}\right)\right], \tag{16}$$

The corresponding non-dimensionless boundary conditions are

$$u = 0, v = 0, \theta = 1, \phi = 1 \text{ at } y = h_1$$
$$u = 0, v = 0, \theta = n \text{ at } y = h_2. \tag{17}$$

Here $h_1 = -1 - \frac{a}{d}\text{Cos}(\frac{2\pi\lambda}{L}x)$ and $h_2 = 1 + \frac{a}{d}\text{Cos}(\frac{2\pi\lambda}{L}x)$.

The local Rayleigh number Ra is defined as $Ra = \frac{(1-C^*)(T_1-T^*)\beta g d_1^3}{\nu\alpha}$, Nr is buoyancy ratio defined by $Nr = \frac{(\rho_p-\rho_f)(C_1-C^*)}{\rho_f\beta(T_1-T^*)(1-C^*)}$, Nb is a Brownian motion defined as $Nb = \frac{\tau D_B(C_1-C^*)}{\alpha}$, Nt is a thermophoresis parameter defined as $Nt = \frac{\tau D_T(T_1-T^*)}{T^*}$ and Ec is the Eckert number defined as $Ec = \frac{c^2}{C_p(T_1-T^*)}$.

In view of the said dimensionless numbers, the Eqs. (13)–(16) for long wave length approximation take the following forms:

$$\frac{\partial u}{\partial x} + \frac{\partial v}{\partial y} = 0, \tag{19}$$

$$\text{Re}\delta\left(u\frac{\partial u}{\partial x} + v\frac{\partial u}{\partial y}\right) = -\frac{\partial p}{\partial x} + \left(\delta^2\frac{\partial^2 u}{\partial x^2} + \frac{\partial^2 u}{\partial y^2}\right) + \frac{Ra}{\text{RePr}}(Nr\phi + \theta), \tag{20}$$

$$\frac{\partial p}{\partial y} = 0, \tag{21}$$

$$\text{RePr}\delta\left(u\frac{\partial\theta}{\partial x} + v\frac{\partial\theta}{\partial y}\right) = \left(\delta^2\frac{\partial^2\theta}{\partial x^2} + \frac{\partial^2\theta}{\partial y^2}\right) + N_b\frac{\partial\phi}{\partial y}\frac{\partial\theta}{\partial y} + N_t\left(\frac{\partial\theta}{\partial y}\right)^2 + E_c\text{Pr}\left(\frac{\partial u}{\partial y}\right)^2, \tag{22}$$

$$\text{Re}\delta\left(u\frac{\partial\phi}{\partial x} + v\frac{\partial\phi}{\partial y}\right) = \frac{1}{S_c}\left[\left(\delta^2\frac{\partial^2\phi}{\partial x^2} + \frac{\partial^2\phi}{\partial y^2}\right) + \frac{N_t}{N_b}\left(\delta^2\frac{\partial^2\theta}{\partial x^2} + \frac{\partial^2\theta}{\partial y^2}\right)\right]. \tag{23}$$

The local Nusselt number along the walls can be expressed as

$$Nu = \frac{dq_w}{K(T_1-T^*)}, \text{ where } q_w = -K\frac{\partial\bar{T}}{\partial\bar{y}} \tag{24}$$

The dimensionless Nusselt number at the wavy wall $y = h_1$ and $y = h_2$ is given by

$$Nu_{h_1} = -\left(\frac{\partial\theta}{\partial y}\right)_{h_1}, Nu_{h_2} = -\left(\frac{\partial\theta}{\partial y}\right)_{h_2} \tag{25}$$

The Sherwood number along the walls can be expressed as

$$Sh = \frac{dq_m}{D_B(C_1-C^*)}, \text{ where } q_m = -D_B\frac{\partial\bar{C}}{\partial\bar{y}} \tag{26}$$

The dimensionless Sherwood number at the wavy wall $y = h_1$ and $y = h_2$ is given by

$$Sh_{h_1} = -\left(\frac{\partial\phi}{\partial y}\right)_{h_1}, Sh_{h_2} = -\left(\frac{\partial\phi}{\partial y}\right)_{h_2} \tag{27}$$

3. Solution of the problem

Here in this section, we utilized the homotopic procedure in order to get the convergent solutions resulting in governing equations. For this purpose the initial guesses and linear operators respectively corresponding to $u(y)$, $\theta(y)$ and $\phi(y)$ respectively are given below:

$$u_0(y) = 0,$$
$$\theta_0(y) = \frac{((1-n)y + (h_1-h_2) - (1-n)h_1)}{h_1-h_2}, \phi_0(y) = \frac{((1-m)y + (h_1-h_2) - (1-m)h_1)}{h_1-h_2}. \tag{28}$$

and

$$\mathcal{L}_1(u) = \frac{d}{dy}\left(\frac{du}{dy}\right), \ \mathcal{L}_2(\theta) = \frac{d}{dy}\left(\frac{d\theta}{dy}\right), \ \mathcal{L}_3(\phi) = \frac{d}{dy}\left(\frac{d\phi}{dy}\right). \tag{29}$$

First we define the following non-linear operators N_1, N_2 and N_3

$$
\left.
\begin{aligned}
N_1[u(y,q),\theta(y,q),\phi(y,q)] &= -P + \frac{\partial^2 u}{\partial y^2} + \frac{Ra}{RePr}(Nr\phi + \theta), \\
N_2[u(y,q),\theta(y,q),\phi(y,q)] &= \frac{\partial^2 \theta}{\partial y^2} + N_b \frac{\partial \phi}{\partial y}\frac{\partial \theta}{\partial y} + N_t\left(\frac{\partial \theta}{\partial y}\right)^2 + E_c \Pr\left(\frac{\partial u}{\partial y}\right)^2, \\
N_3[u(y,q),\theta(y,q),\phi(y,q)] &= \frac{\partial^2 \phi}{\partial y^2} + \frac{N_t}{N_b}\frac{\partial^2 \theta}{\partial y^2}.
\end{aligned}
\right\}
\tag{30}
$$

and then construct the homotopy

$$
\left.
\begin{aligned}
(1-q)\pounds_1[u(y,q)-u_0(y)] &= q\hbar N_1[u(y,q),\theta(y,q),\phi(y,q)], \\
(1-q)\pounds_2[\theta(y,q)-\theta_0(y)] &= q\hbar N_2[u(y,q),\theta(y,q),\phi(y,q)], \\
(1-q)\pounds_3[\phi(y,q)-\phi_0(y)] &= q\hbar N_3[u(y,q),\theta(y,q),\phi(y,q)],
\end{aligned}
\right\}
\tag{31}
$$

where $\hbar$ is convergence control parameter.

For $q = 0$

$$
u(y,0) = u_0(y), \theta(y,0) = \theta_0(y), \phi(y,0) = \phi_0(y)
\tag{32}
$$

For $q = 1$

$$
u(y,1) = u(y), \theta(y,1) = \theta(y), \phi(y,1) = \phi(y)
\tag{33}
$$

When embedding parameter q diverges from 0 to 1, then $f(y,q)$, $\theta(y,q)$ and $\phi(y,q)$ varies from initial guess $u_0(y)$, $\theta_0(y)$ and $\phi_0(y)$ to final $u(y)$, $\theta(y)$ and $\phi(y)$ solution.

Let us expand $u(y,q)$, $\theta(y,q)$ and $\phi(y,q)$ in Maclaurin's series as

$$
\left.
\begin{aligned}
u(y,q) &= u_0(y) + \sum_{l=1}^{\infty} u_l(y) q^l, \\
\theta(y,q) &= \theta_0(y) + \sum_{l=1}^{\infty} \theta_l(y) q^l, \\
\phi(y,q) &= \phi_0(y) + \sum_{l=1}^{\infty} \phi_l(y) q^l.
\end{aligned}
\right\}
\tag{34}
$$

In which

$$
u_l(y) = \frac{1}{l!}\frac{\partial^l u(y,q)}{\partial q^l}\bigg|_{q=0}, \theta_l(y) = \frac{1}{l!}\frac{\partial^l \theta(y,q)}{\partial q^l}\bigg|_{q=0}, \phi_l(y)
$$
$$
= \frac{1}{l!}\frac{\partial^l \phi(y,q)}{\partial q^l}\bigg|_{q=0}.
\tag{35}
$$

Differentiating $l-$ times to zeroth-order deformation Eq. (31) with respect to the q and dividing it by $l!$ then putting $q = 0$ and gain $lth-$order deformation expression for $u_l(y)$, $\theta_l(y)$ and $\phi_l(y)$ as follow

$$
\left.
\begin{aligned}
\pounds_1[u_l(y) - \chi_l u_{l-1}(y)] &= \hbar_1 Ru_l(y), \\
\pounds_2[\theta_l(y) - \chi_l \theta_{l-1}(y)] &= \hbar_2 R\theta_l(y), \\
\pounds_3[\phi_l(y) - \chi_l \phi_{l-1}(y)] &= \hbar_3 R\phi_l(y),
\end{aligned}
\right\}
\tag{37}
$$

$$
\left.
\begin{aligned}
u_l(y,q) = 0, \ \theta_l(y,q) = 1, \ \phi_l(y,q) = 1 \text{ at } y = h_1 \\
u_l(y,q) = 0, \ \theta_l(y,q) = n, \ \phi_l(y,q) = m \text{ at } y = h_2
\end{aligned}
\right\},
\tag{38}
$$

$$
\left.
\begin{aligned}
Ru_l(y) &= -P + u_l'' + \frac{Ra}{RePr}(Nr\phi_l + \theta_l), \\
R\theta_l(y) &= \theta_l'' + N_b\sum_{k=0}^{l}\theta_k'\phi_{l-k}' + N_t\sum_{k=0}^{l}\theta_k'\theta_{l-k}' + E_c \Pr\sum_{k=0}^{l}u_k'u_{l-k}', \\
R\phi_l(y) &= \phi_l'' + \frac{N_t}{N_b}\theta_l''.
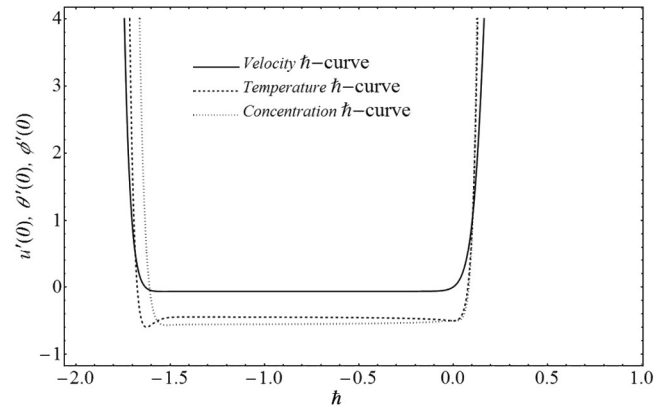\end{aligned}
\right\}
\tag{39}
$$

Fig. 2. $\hbar$-Curves for velocity, temperature and concentration upto 30th-order approximations.

The $lth-$order approximation of the solution can be expressed as

$$
\left.
\begin{aligned}
u(y) &= u_0(y) + \sum_{k=1}^{l} u_k(y), \\
\theta(y) &= \theta_0(y) + \sum_{k=0}^{l} \theta_k(y), \\
\phi(y) &= \phi_0(y) + \sum_{k=0}^{l} \phi_k(y).
\end{aligned}
\right\}
\tag{40}
$$

The solutions expressions for the best understanding of readers at first and second iterations for velocity, temperature and concentration are given as

$$
u = \frac{3}{8} - \frac{1}{40}y - \frac{3}{8}y^2 + \frac{1}{40}y^3 + N_r\left(\frac{3}{40} - \frac{1}{40}y - \frac{3}{40}y^2 + \frac{1}{40}y^3\right),
\tag{41}
$$

$$
\theta = \frac{1}{2} - \frac{1}{2}y + N_b\left(\frac{3}{40} - \frac{3}{40}y^2\right) + N_t\left(\frac{3}{40} - \frac{3}{40}y^2\right),
\tag{42}
$$

$$
\phi = \frac{1}{2} - \frac{1}{2}y.
\tag{43}
$$

and

$$
u = \frac{33}{40} - \frac{7}{200}y - \frac{33}{40}y^2 + \frac{7}{200}y^3 + N_r\left(
\begin{aligned}
&\frac{21}{200} - \frac{7}{200}y - \frac{21}{200}y^2 + \frac{7}{200}y^3 + \\
&N_b\left(\frac{3}{320} - \frac{9}{800}y^2 + \frac{3}{1600}y^4\right) + \\
&N_t\left(\frac{3}{320} - \frac{9}{800}y^2 + \frac{3}{1600}y^4\right)
\end{aligned}
\right),
\tag{44}
$$

Table 1
Residual error when $\phi = 2\%$, $N_t = N_b = N_r = 0.5$, and $Pr = 10$.

Order of approximation	$u(y)$	$\theta(y)$	$\phi(y)$
2	4.297×10^{-2}	3.633×10^{-3}	2.323×10^{-4}
6	2.124×10^{-5}	2.165×10^{-6}	1.743×10^{-7}
10	2.229×10^{-6}	1.912×10^{-7}	1.443×10^{-8}
14	5.176×10^{-7}	1.221×10^{-10}	3.561×10^{-8}
18	3.533×10^{-12}	3.741×10^{-12}	3.767×10^{-13}
20	2.669×10^{-14}	2.884×10^{-15}	3.324×10^{-14}

Table 2
Correlation between homotopic solutions by $\hbar$-curve and optimal series solution using GA and NM for velocity u.

N_b	N_t	N_r	L_e	Series solution			Optimal solution with GA and NM			
				Iteration	Time	Error	Iteration	Time	$\hbar$-curves	Error
0.3	0.3	0.3	1	10	2.567	1.6×10^{-1}	10	0.099	-0.612730	5.6×10^{-3}
				20	90.623	4.0×10^{-3}	20	1.212	-0.591276	4.3×10^{-6}
				30	301.426	7.9×10^{-5}	30	5.339	-0.612730	7.3×10^{-8}
0.4	0.4	0.4	2	10	2.837	1.6×10^{-1}	10	0.212	-0.586543	2.2×10^{-3}
				20	93.742	4.0×10^{-3}	20	1.534	-0.736722	5.4×10^{-5}
				30	310.237	7.9×10^{-5}	30	5.644	-0.612730	7.3×10^{-8}
0.5	0.5	0.5	3	10	2.977	1.6×10^{-1}	10	0.411	-0.839433	7.1×10^{-2}
				20	95.123	4.0×10^{-3}	20	1.722	-0.735678	4.3×10^{-6}
				30	312.123	7.9×10^{-5}	30	5.892	-0.612730	6.4×10^{-8}

$$\theta = \frac{1}{2} - \frac{1}{2}y + N_t\left(\frac{21}{200} - \frac{21}{200}y^2\right) + N_t^2\left(\frac{3}{200}y - \frac{3}{200}y^3\right) + N_b^2\left(\frac{3}{400}y - \frac{3}{400}y^3\right) +$$
$$N_b\left(\frac{21}{200} + \frac{9}{400}N_t y - \frac{21}{200}y^2 - \frac{9}{400}N_t y^3\right),$$

$$(45)$$

$$\phi = \frac{1}{N_b}\left(N_t^2\left(-\frac{9}{200} + \frac{9}{200}y^2\right) + N_b\left(\frac{1}{2} - \frac{1}{2}y + N_t\left(-\frac{9}{200} + \frac{9}{200}y^2\right)\right)\right).$$

$$(46)$$

4. Convergence of the solutions

The homotopic method gives us an amazing adaptability to pick the auxiliary parameter $\hbar$. As pointed out by Liao [31], the rate of approximation and the convergence region is dependent on $\hbar$. To decide the appropriate value of $\hbar$, Fig. 2 portrays the $\hbar$-curves to find the permissible values for interval of convergence for velocity, temperature and concentration. The admissible ranges for velocity profile, temperature profile and nanoparticle concentration are $-1.6 \leq \hbar \leq -0.1$, $-1.5 \leq \hbar \leq -0.4$ and $-1.5 \leq \hbar \leq -0.1$ respectively.

Moreover, the error of norm 2 of two successive approximations for velocity, temperature and concentration over [0,1] with HAM by 30th-order approximations are calculated by

$$E_u = \sqrt{\frac{1}{21}\sum_{i=0}^{15}(u(i/20))^2},$$
$$E_\theta = \sqrt{\frac{1}{21}\sum_{i=0}^{15}(\theta(i/20))^2}, \quad \left. \right\}$$
$$E_\phi = \sqrt{\frac{1}{21}\sum_{i=0}^{15}(\phi(i/20))^2}.$$

$$(41)$$

It is seen that the error is minimum at $\hbar = -0.6$ for velocity, temperature and concentration as shown in Table 1. It is also noteworthy that the admissible values $\hbar$ lie in their respective admissible range.

A hybrid Genetic Algorithm and Nelder-Mead approach [32] is also used to accelerate homotopy technique to find the value of embedding parameter $\hbar$. Detail is given in the following numerical Tables 2 to 5.

Table 3
Correlation between homotopic solutions by $\hbar$-curve and optimal series solution using GA and NM for temperature θ.

N_b	N_t	N_r	L_e	Series solution			Optimal solution with GA and NM			
				Iteration	Time	Error	Iteration	Time	$\hbar$-curves	Error
0.3	0.3	0.3	1	10	2.567	1.8×10^{-2}	10	0.099	-0.612730	6.5×10^{-5}
				20	90.623	4.2×10^{-4}	20	1.212	-0.638747	5.3×10^{-7}
				30	301.426	7.9×10^{-7}	30	5.339	-0.839930	7.7×10^{-9}
0.4	0.4	0.4	2	10	2.837	1.7×10^{-2}	10	0.212	-0.653733	2.2×10^{-5}
				20	93.742	4.4×10^{-5}	20	1.534	-0.783722	6.5×10^{-7}
				30	310.237	7.9×10^{-7}	30	5.644	-0.867330	7.8×10^{-9}
0.5	0.5	0.5	3	10	2.977	1.8×10^{-3}	10	0.411	-0.638933	7.9×10^{-4}
				20	95.123	4.3×10^{-5}	20	1.722	-0.735678	4.8×10^{-7}
				30	312.123	7.5×10^{-7}	30	5.892	-0.666730	6.9×10^{-9}

Table 4
Correlation between homotopic solutions by $\hbar$-curve and optimal series solution using GA and NM for concentration ϕ.

N_b	N_t	N_r	L_e	Series solution			Optimal solution with GA and NM			
				Iteration	Time	Error	Iteration	Time	$\hbar$-curves	Error
0.3	0.3	0.3	1	10	2.567	2.4×10^{-2}	10	0.099	-0.612730	5.3×10^{-5}
				20	90.623	8.4×10^{-4}	20	1.212	-0.867476	4.3×10^{-7}
				30	301.426	9.9×10^{-6}	30	5.339	-0.873660	3.3×10^{-9}
0.4	0.4	0.4	2	10	2.837	1.6×10^{-2}	10	0.212	-0.654783	2.2×10^{-5}
				20	93.742	4.7×10^{-4}	20	1.534	-0.778332	5.7×10^{-7}
				30	310.237	7.9×10^{-6}	30	5.644	-0.765333	2.3×10^{-9}
0.5	0.5	0.5	3	10	2.977	1.9×10^{-2}	10	0.411	-0.646747	5.5×10^{-4}
				20	95.123	4.1×10^{-4}	20	1.722	-0.767678	4.3×10^{-7}
				30	312.123	$7.3 \times 10^{-}$	30	5.892	-0.648430	3.2×10^{-9}
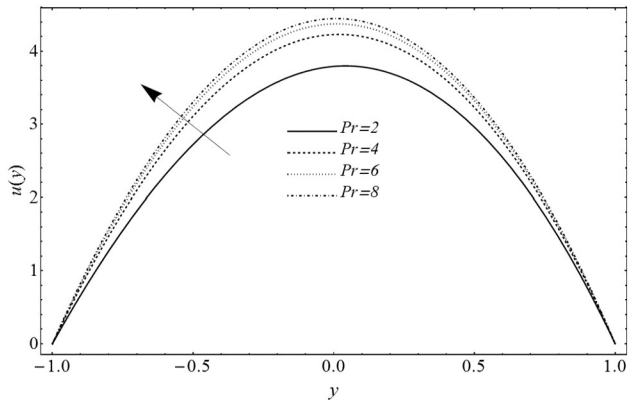
Fig. 3. The dimensionless velocity profiles for various values of Pr with $Nr = Nt = Nb = 0.5$.

Fig. 6. The dimensionless streamlines.

5. Results and discussion

To see the effects of emerging parameters on velocity, temperature, nanoparticle concentration, Nusselt number, skin-friction coefficient and Sherwood number Figs. 3 to 16 have been displayed. To get better understanding of flow and heat transfer characteristics in the nanofluid, we thereafter make a detailed analysis on the problem of the fully developed nanofluid flow and heat transfer in a horizontal channel. The dimensionless velocity profiles $u(y)$ for various values of Pr when $Nr = Nt = Nb = 0.5$ are presented in Fig. 3. It can be seen that for Prandtl number, the velocity near the centerline of the channel increases by increasing the values of Pr while it decreases near the walls with the increasing magnitude of Pr. It is in accordance with the physical expectation, because it is due to the fact that, viscous force near the walls, plays an important role to keep the fluid attached with the walls, therefore, increasing of Buoyancy force immediately yields an increase in the velocity profile. The dimensionless velocity profile for various values of Nr are presented in Fig. 4 for the fixed $Nt = Nb = 0.5$ and $Pr = 10$. It is
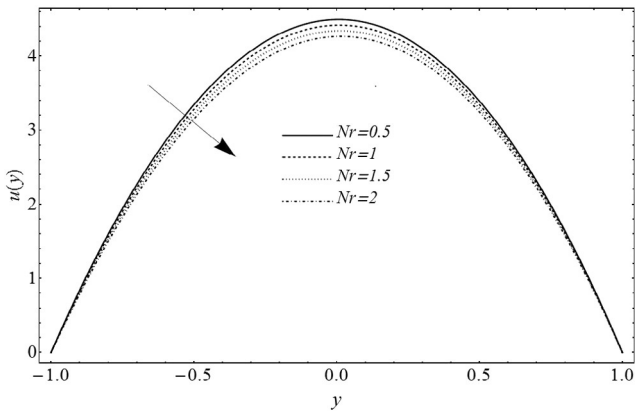
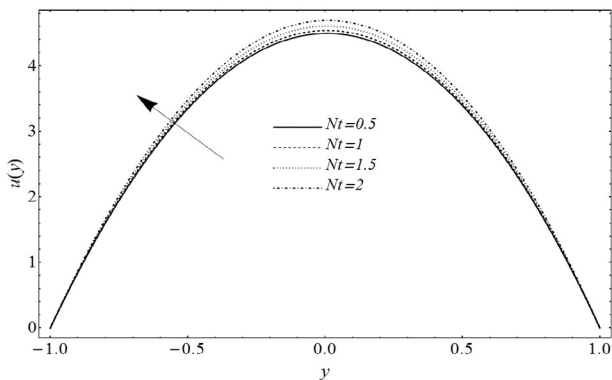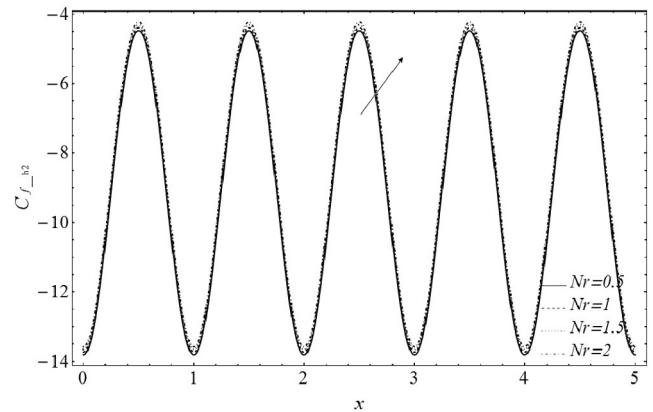Fig. 4. The dimensionless velocity profiles for various values of Nr with $Nt = Nb = 0.5$ and

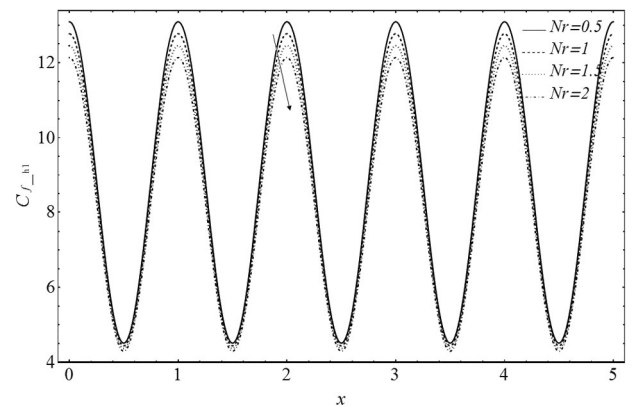Fig. 5. The dimensionless velocity profiles for various values of Nt with $Nr = Nb = 0.5$ and $Pr = 10$.

Fig. 7. (bottom). The dimensionless skin friction for various values of Nr with $Nt = Nb = 0.5$ and $Pr = 10$. (top). The dimensionless skin friction for various values of Nr with $Nt = Nb = 0.5$ and $Pr = 10$.
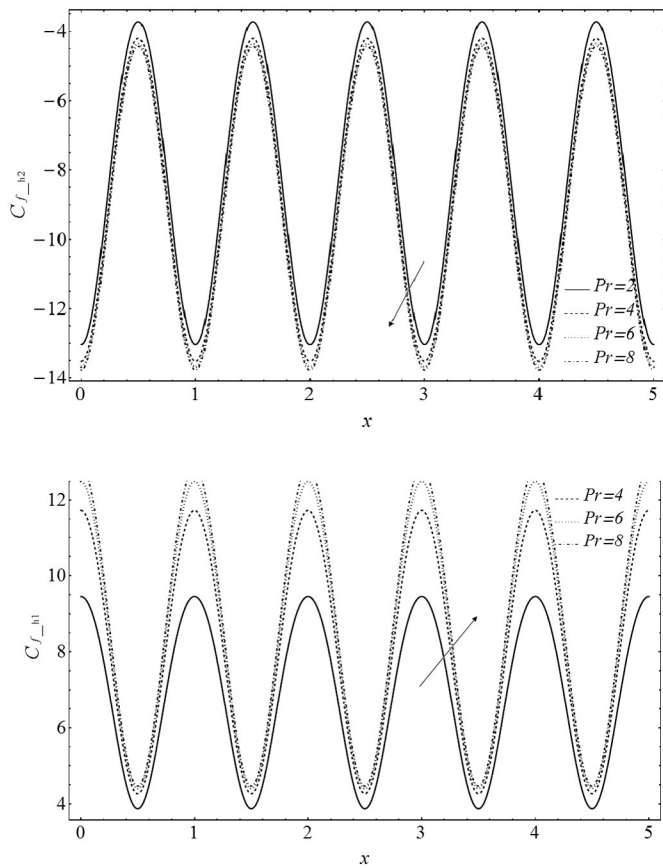
Fig. 8. (bottom). The dimensionless skin friction for various values of Pr with $Nt=Nb=Nr=0.5$. (bottom). The dimensionless skin friction for various values of Pr with $Nt=Nb=Nr=0.5$.
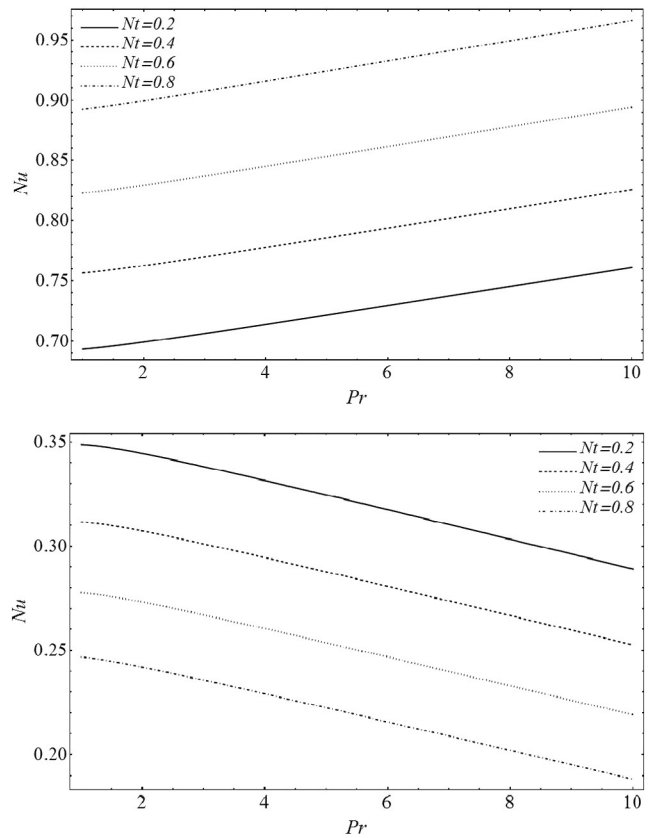

Fig. 9. (bottom). Effects of Prandtl number and thermophoresis parameters on temperature for various values of Nt with $Nr=Nb=0.5$ and $Pr=10$. (top) Effects of Prandtl number and thermophoresis parameters on temperature for various values of Nt with $Nr=Nb=0.5$ and $Pr=10$.

found that for Buoyancy ratio case ($Nr>0$), the velocity near the centerline of the channel decreases with the increase of Nr while in the vicinity of the walls it decreases. The dimensionless velocity profile for various values of Nt with $Nr=Nb=0.5$ and $Pr=10$ are presented in Fig. 5. It can be seen from Fig. 5 that for thermophoresis parameter case ($Nt>0$), the dimensionless velocity near the centerline of the channel decreases by increase the values of Nt while in the vicinity of the walls it decreases endlessly with the magnitude of Nt. Fig. 6 displays the streamlines. Fig. 7 shows the effects of skin fiction with the different Buoyancy ratio Nr with $Nt=Nb=0.5$ and $Pr=10$. In Fig.7— (top), it is found that skin fiction increases with the increase of the Buoyancy ratio whereas at bottom, skin fiction decreases by increasing the values of Buoyancy ratio. Fig. 8— (top) and (bottom) show the effects of skin fiction with the different Prandtl number Pr when $Nr=Nt=Nb=0.5$ are kept fixed. It can be noted that in Fig. 8— (top), the skin fiction decreases with increasing the Prandtl number while in Fig. 8— (bottom), skin fiction increases with increasing the Prandtl number. Fig. 9— (top) and (bottom) shows the effects of Nusselt number with the different thermophoresis parameters Nt with $Nr=Nb=0.5$ and $Pr=10$. It can be seen at the top of Fig. 9, that Nusselt number decreases by increasing the values of thermophoresis parameters while at the bottom of Fig. 9, the Nusselt number increases with the increase of thermophoresis parameters. The temperature profile $\theta(y)$ for various values of Pr with $Nr=Nt=Nb=0.5$ is offered in Fig. 10. It is revealed that the temperature in the channel increases monotonously with the increase of Pr. Fig. 11— (top) and (bottom) shows variation of Nusselt number along the wavy channel for different values of Prandtl number. As shown in these figures, the Nusselt number has a rapid reduction from the channel inlet plane until the core flow meets the bumps on the channel throats. As the flow moves downstream, when the channel

cross-sectional areas over the bumps (or the throats) decreases, the average velocity at the section and as a result the corresponding velocity gradient increases, subsequently, a salient in the Nusselt number is experienced over the channel throats. It is also noted in Fig. 11— (top), when the Prandtl number Pr increases, the Nusselt number Nu decreases at the peak and the minimum values of the Nusselt number occur slightly upstream of the maximum cross sections of the channel. Fig. 11 (bottom) shows the profile of the Nusselt number along the wavy channel at various values of Prandtl number Pr. It is exposed that it increases with the increase in the Prandtl number. Fig. 12 shows the variation of Nusselt number along the wavy channel for
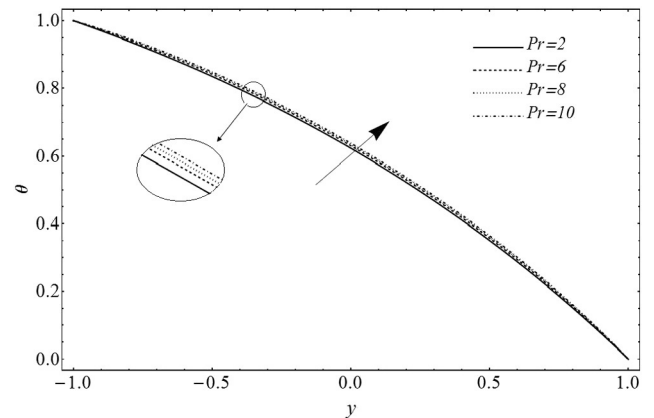

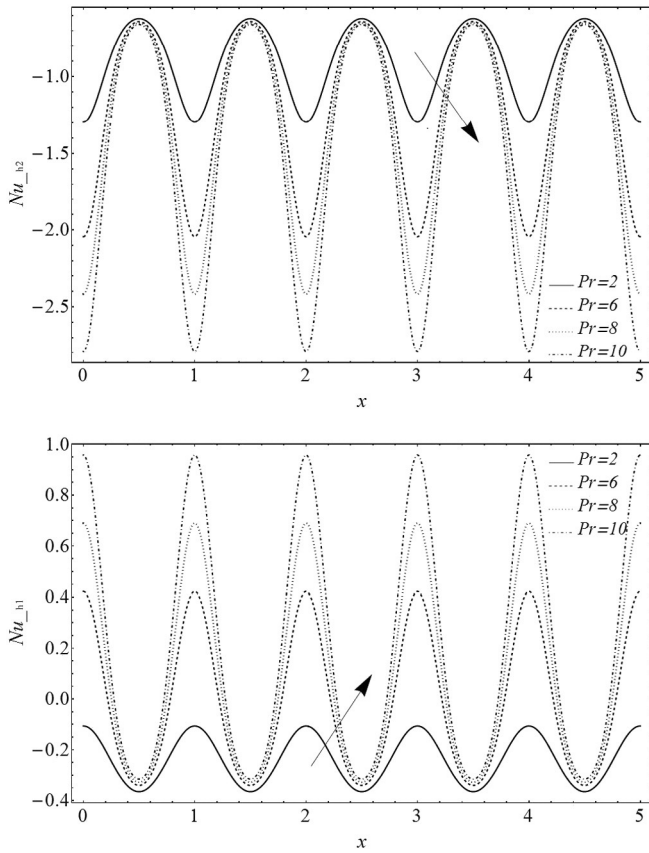Fig. 10. The dimensionless temperature profiles for various values of Pr with $Nr=Nt=Nb=0.5$.

Fig. 11. (bottom). Effects of Prandtl number on distribution of Nusselt number. (top) Effect of Prandtl number on distribution of Nusselt number.

Fig. 13. (bottom). Nanoparticle volume fraction profiles for various values of Nt with $Nr = Nb = 0.5$ and $Pr = 10$. (top) Nanoparticle volume fraction profiles for various values of Nt with $Nr = Nb = 0.5$ and $Pr = 10$.

different values of Prandtl number. As shown in these figures, the Nusselt number increases by increasing the Prandtl number at the top of the channel and Nusselt number decreases by increasing the Prandtl number at the bottom of the channel. Fig. 13— (top) and (bottom) demonstrates the effects of Nusselt number with the different thermophoresis parameters Nt with $Nr = Nb = 0.5$ and $Pr = 10$. It is discovered at the top that Nusselt number increases with increasing values of thermophoresis parameter however at the bottom, Nusselt number increases with increasing values of thermophoresis parameters. The dimensionless nanoparticle volume fraction profiles $\varphi(y)$ for various values of Pr with $Nr = Nt = Nb = 0.5$ are accessible in Fig. 14. It is seen that for Prandtl number case ($Pr > 0$), the dimensionless nanoparticle volume fraction in the channel decreases monotonously with the
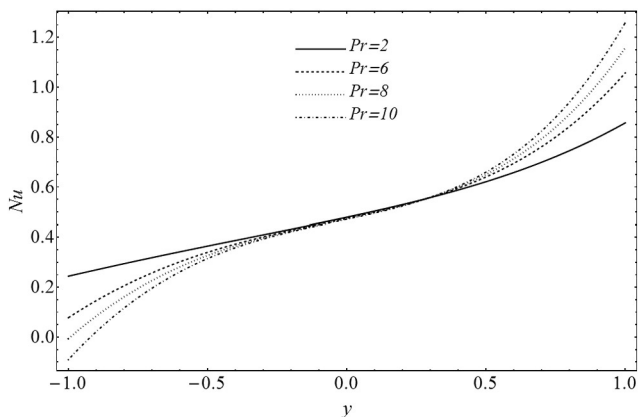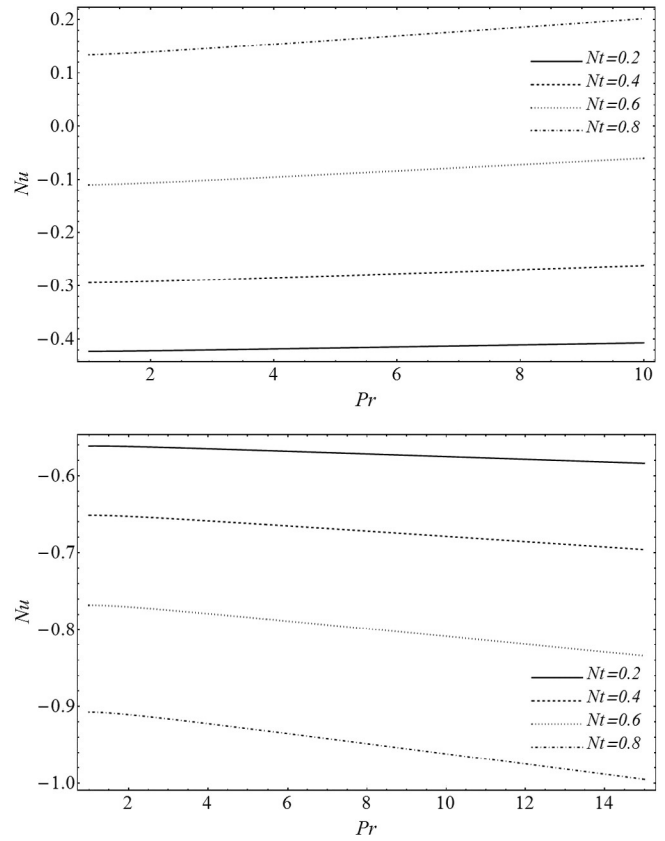
increase of Pr Fig. 15— (top) and (bottom) show the variation of Sherwood number Sh along the wavy channel for different values of Prandtl number. It is depicted that the Sherwood number Sh has a rapid reduction from the channel inlet plane until the core flow meets the bumps on the channel throats. As the flow moves downstream, when the channel cross-sectional areas over the bumps (or the throats) decrease, the average velocity at the section, and the corresponding velocity gradient increase obviously. Consequently a salient in the Sherwood number Sh is experienced over the channel throats. In Fig. 15— (top), it is noticed that when the Prandtl number Pr increases, the peak value of the Sherwood number Sh increases as well. The minimum values of the Sherwood number Sh occur slightly upstream of the maximum cross
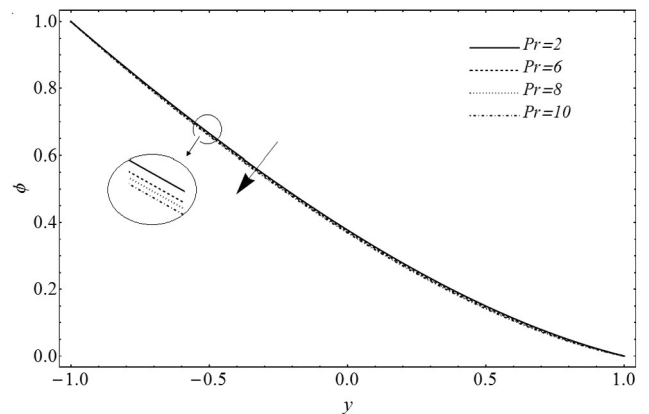

Fig. 12. Effect of Prandtl number on distribution of Nusselt number.

Fig. 14. The dimensionless nanoparticle volume fraction profiles for various values of Pr with $Nr = Nt = Nb = 0.5$.
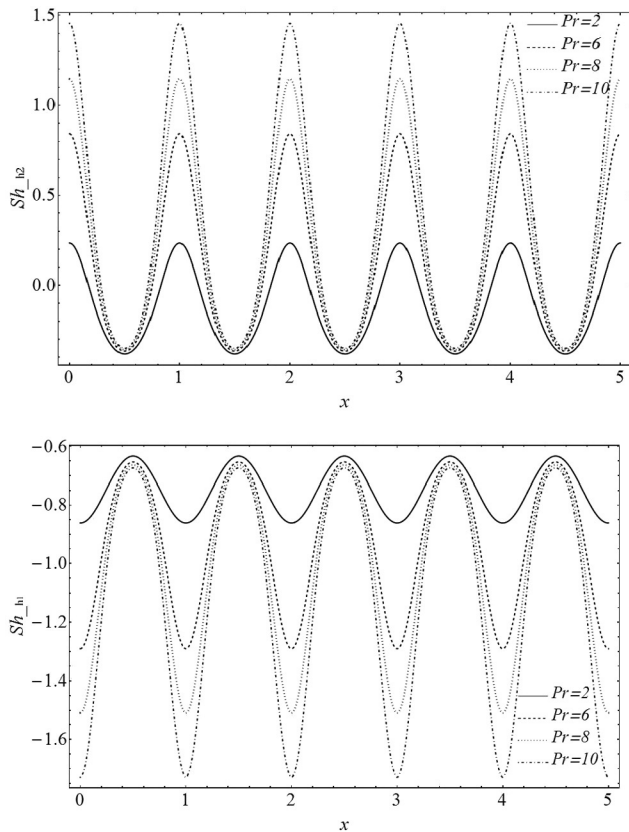
Fig. 15. (bottom) Effects of Prandtl number on distribution of Sherwood number. (top) Effects of Prandtl number on distribution of Sherwood number.

sections of the channel. Fig. 15— (bottom) shows the profile of the Sherwood number Sh along the wavy channel at various values of Prandtl number Pr. Sherwood number decreases with increasing values of Prandtl number. Fig. 16 shows the variation of Sherwood number Sh along the wavy channel for different values of Prandtl number. The Sherwood number Sh increases by increasing the Prandtl number at the top of the channel while it decreases by increasing the Prandtl number at the bottom of the channel.

Pr = 10.

6. Conclusions

In this paper, effects of convective heat transfer of nanofluid in a wavy channel are reported. Constant pressure gradient is taken into account. Effects of different parameters on velocity, temperature,
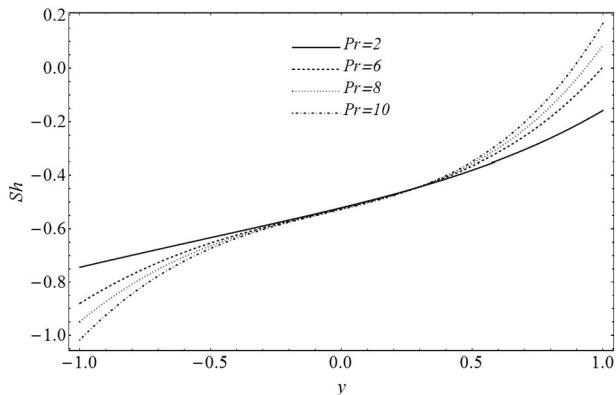

Fig. 16. Effects of Sherwood number.

nanoparticle volume fraction, Nusselt numbers and Sherwood number are examined graphically. Numerical results are presented for the convergence of series solutions. It is observed that the velocity near the centerline of the channel monotonously increases with the increase of Prandtl number and thermophoresis parameter while it decreases in the vicinity of the walls. On the other hand velocity near the centerline of the channel decreases by increasing the Buoyancy ratio whereas in the vicinity of the walls velocity decreases with the increasing magnitude of Buoyancy ratio. The dimensionless temperature in the channel increases with the increase of Pr but quite the reverse behavior is noted for the case of dimensionless nanoparticle volume fraction. The nanoparticle volume fraction in the channel decreases with the increase of Pr. Nusselt number is also increasing function of Pr. It is also noted that the Sherwood number and Nusselt number decrease with the increase of Pr at the bottom of the channel while Sherwood number is increased with the increase of Pr at the top of the channel.

Acknowledgment

References

[1] S.U.S. Choi, J.A. Eastman, Enhancing thermal conductivity of fluids with nanoparticles in: the proceedings of the ASME international mechanical engineering congress and exposition, ASME, San Franc. 66 (1995) 99–105.

[2] Y. Rao, Nanofluids: stability, phase diagram, rheology and applications, Particuology 8 (2010) 549–555.

[3] M. Sheikholeslami, D.D. Ganji, Heat transfer of Cu–water nanofluid flow between parallel plates, Powder Technol. 235 (2013) 873–879.

[4] K. Milani Shirvan, M. Mamourian, S. Mirzakhanlari, R. Ellahi, Two phase simulation and sensitivity analysis of effective parameters on combined heat transfer and pressure drop in a solar heat exchanger filled with nanofluid by RSM, J. Mol. Liq. 220 (2016) 888–901.

[5] R. Ellahi, A. Zeeshan, M. Hassan, Shape effects of nanosize particles in Cu-H₂0 nanofluid on entropy generation, Int. J. Heat Mass Transf. 81 (2015) 449–456.

[6] M. Sheikholeslami, D.D. Ganji, Entropy generation of nanofluid in presence of magnetic field using Lattice Boltzmann Method, Physica A 417 (2015) 273–286.

[7] O. Mahian, A. Kianifar, S.A. Kalogirou, I. Pop, S. Wongwises, A review of the applications of nanofluids in solar energy, Int. J. Heat Mass Transf. 57 (2013) 582–594.

[8] S. Ahmad, A.M. Rohni, I. Pop, Blasius and Sakiadis problems in nanofluids, Acta Mech. 218 (2011) 195–204.

[9] S.T. Mohyud-Din, Z.A. Zaidi, U. Khan, N. Ahmed, On heat and mass transfer analysis for the flow of a nanofluid between rotating parallel plates, Aerosp. Sci. Technol. 46 (2015) 514–522.

[10] N. Ahmed, S.T. Mohyud-Din, S.M. Hassan, Flow and heat transfer of nanofluid in an asymmetric channel with expanding and contracting walls suspended by carbon nanotubes: a numerical investigation, Aerosp. Sci. Technol. 48 (2016) 53–60.

[11] S.T. Mohyud-Din, U. Khan, N. Ahmed, S.M. Hassan, Magnetohydrodynamic flow and heat transfer of nanofluids in stretchable convergent/divergent channels, Appl. Sci. 5 (2015) 1639–1664.

[12] R. Ellahi, M. Hassan, A. Zeeshan, Shape effects of nanosize particles in Cu-H₂O nanofluid on entropy generation, Int. J. Heat Mass Transf. 81 (2015) 449–456.

[13] R. Ellahi, S.U. Rahman, S. Nadeem, Blood flow of Jeffrey fluid in a Catherized tapered artery with the suspension of nanoparticles, Phys. Lett. A 378 (2014) 2973–2980.

[14] N.S. Akbar, Ferromagnetic CNT Suspended H₂O + Cu Nanofluid Analysis through Composite Stenosed Arteries with Permeable Wall, Physica E: Low-Dimensional Systems and Nanostructures, 72, 2015, pp. 70–76.

[15] R. Ellahi, M. Hassan, A. Zeeshan, A.A. Khan, Shape effects of nanoparticles suspended in HFE-7100 over wedge with entropy generation and mixed convection, Appl. Nanosci. 6 (2016) 641–651.

[16] R. Ellahi, M. Hassan, A. Zeeshan, Aggregation effects on water base Al₂O₃ nanofluid over permeable wedge in mixed convection, Asia Pac. J. Chem. Eng. 11 (2016) 179–186.

[17] S. Soleimani, M. Sheikholeslami, D.D. Ganji, M. Gorji-Bandpay, Natural convection heat transfer in a nanofluid filled semi-annulus enclosure, Int. Commun. Heat Mass Transf. 39 (2012) 565–574.

[18] M. Sheikholeslami, R. Ellahi, Three dimensional mesoscopic simulation of magnetic field effect on natural convection of nanofluid, Int. J. Heat Mass Transf. 89 (2015) 799–808.

[19] R.K. Nayak, S. Bhattacharyya, I. Pop, Numerical study on mixed convection and entropy generation of a nanofluid in a lid-driven square enclosure, J. Heat Transf. 138 (2016) (012503-1-11).

[20] S. Soleimani, M. Sheikholeslami, D.D. Ganji, M. Gorji-Bandpay, Natural convection heat transfer in a nanofluid filled semi-annulus enclosure, Int. Commun. Heat Mass Transf. 39 (2012) 565–574.

[21] S. Zeinali Heris, M. Nasr Esfahany, S.G. Etemad, Numerical investigation of nanofluid laminar convective heat transfer through circular tube, J. Numer. Heat Transf., Part A: Appl. 52 (2007) 1043–1058.

[22] S. Lee, S.U.S. Choi, S. Li, J.A. Eastman, Measuring thermal conductivity of fluids containing oxide nanoparticles, J. Heat Transf. 121 (1999) 280–289.

[23] Y. Xuan, Q. Li, Heat transfer enhancement of nanofluids, Int. J. Heat Fluid Flow 21 (2000) 58–64.

[24] Y. Xuan, Q. Li, Investigation on convective heat transfer and flow features of nanofluids, J. Heat Transf. 125 (2003) 151–155.

[25] A.K. Santra, S. Sen, N. Charaborty, Study of heat transfer due to laminar flow of copper- water nanofluid through two isothermally heated parallel plates, Int. J. Therm. Sci. 48 (2009) 391–400.

[26] N.S. Akbar, Nanofluid analysis for the intestinal flow in a symmetric channel, IEEE Trans. Nano Bio. Sci. 13 (2014) 392–396.

[27] S.J. Liao, The Proposed Homotopy Analysis Technique for the Solution of Nonlinear Problems(Ph.D. dissertation) Shanghai Jiao Tong University, Shanghai, China, 1992.

[28] S. Nadeem, A. Hussain, MHD flow of a viscous fluid on a nonlinear porous shrinking sheet by homotopy analysis method, Appl. Math. Mech. 30 (2009) 1569–1578.

[29] J. Buongiorno, Convective transport in nanofluids, ASME J. Heat Transf. 128 (2006) 240–250.

[30] A.V. Kuznetsov, D.A. Nield, Natural convective boundary-layer flow of a nanofluid past a vertical plate, Int. J. Therm. Sci. 49 (2010) 243–247.

[31] S.J. Liao, Beyond Perturbation: Introduction to Homotopy Analysis Method, Chapman & Hall, Boca Raton, 2003.

[32] N.E. Mastorakis, Numerical Solution of Non-Linear Ordinary Differential Equations via Collocation Method (Finite Elements) and Genetic Algorithms, Proceedings of the 6th WSEAS Int, Confer. on Evolu. Comput, Lisbon, Portugal, 2005.